ARTICLE

Preparation of Core/Shell and Hollow Nanostructures of Cerium Oxide by Electrodeposition on a Polystyrene Sphere Template

Ippei Yamaguchi,[†] Mitsuru Watanabe,*[,‡] Tsutomu Shinagawa,[†,‡] Masaya Chigane,[‡] Minoru Inaba,[†] Akimasa Tasaka,[†] and Masanobu Izaki[§]

Department of Applied Chemistry, Graduate School of Engineering, Doshisha University, Kyoto 610-0321, Japan, Electronic Materials Research Division, Osaka Municipal Technical Research Institute, Osaka 536-8553, Japan, and Department of Production System Engineering, Toyohashi University of Technology, Toyohashi, Aichi 441-8580, Japan

ABSTRACT Core/shell nanostructures of polystyrene (PS)/CeO_2 have been prepared on conductive glass substrates by using a novel electrochemical route consisting of (i) the electrophoretic deposition of a PS sphere monolayer on the substrate and (ii) the following potentiostatic electrodeposition of CeO_2 on the PS sphere template in $Ce(NO_3)_3$ aqueous solutions. The structural morphologies of the deposit changed drastically depending on the $Ce(NO_3)_3$ concentration; i.e., spherical and needlelike shells were deposited. The deposit was formed only on the PS sphere surface because of an interaction between cationic cerium species and a sulfate group that was immobilized on the PS sphere surface. The spherical shell layer was assigned as CeO_2, and the needlelike shells were composed of $Ce(OH)_3$ needles formed on the CeO_2 layer surface, indicating that the deposit species changes from CeO_2 to $Ce(OH)_3$ during electrodeposition only in a 1 mM Ce^{3+} solution. Deposition of $Ce(OH)_3$ would begin when electrogenerated hydrogen peroxide was consumed by decomposition under reductive conditions and could no longer oxidize Ce^{3+} ions. The corresponding CeO_2 hollow shells were obtained by thermal elimination of the PS sphere core and transformation of $Ce(OH)_3$ into CeO_2 while keeping their original shapes.

KEYWORDS: CeO_2 • electrodeposition • PS sphere template • core/shell nanostructure

INTRODUCTION

Cerium dioxide (CeO_2) has been successfully employed in technological applications, including polishing materials (1), catalysts (2), oxygen sensors (3), and UV-blocking filters (4), because of its high refractive index, chemical stability, mechanical hardness, high dielectric constant, and high transparency in the visible and near-IR region. Especially, its high photo- and thermocatalytic activities are attractive as an anode material for photoelectrolysis of water (5) and fuel cells (6), respectively. To enhance the performance in the above applications, CeO_2 with a wide range of geometries, such as a continuous layer, particles of nanocube (7), nanorod (8), and nanotube (9), and an inverse opal thin film and powder (10), has been proposed.

Core/shell and hollow nanostructures are widely considered as an effective structure for applications in high-surface-area catalysts (11), high-efficiency photodecomposition agents (12), and low-density batteries or devices (13). Although hollow nanoparticles of CoOOH and CeO_2 have been prepared by a self-assembled synthesis using hydrothermal treatment (14), it is very difficult to control the shape and to obtain nanostructures directly attached on a substrate. Recently, we have developed a novel electrochemical route for the preparation of polystyrene (PS)/ZnO core/shell nanocauliflower arrays on conductive glass substrates, in which anionic PS spheres deposited electrophoretically on the substrate were used as a template (core) for the electrodeposition of ZnO (15). Electrophoretic deposition (EPD) and electrodeposition were performed by using an aqueous suspension of the PS spheres and an aqueous solution of $Zn(NO_3)_2$, respectively. The surface of the PS spheres was functionalized with a sulfate group and has a negative charge that makes the monolayered PS sphere template without aggregation possible. In addition, the interaction between the sulfate group and Zn^{2+} cations, which has been confirmed by XPS analysis, leads to site-selective ZnO deposition, resulting in the ZnO nanopillar shell grown radially from the PS spheres. By means of electrodeposition, the quality, morphology, and size of metal oxide crystals are easily controlled by variation in the reaction potential, amount of electric charge, and concentration of the reactant. This method, therefore, potentially offers a simple and large scalable route to obtain a variety of nanostructures composed of a PS sphere core and an inorganic shell on a substrate. Furthermore, the inorganic hollow shell can be readily obtained by thermal elimination of the PS core.

* Corresponding author. E-mail: watanabe@omtri.city.osaka.jp.
Received for review January 20, 2009 and accepted April 13, 2009
[†] Doshisha University.
[‡] Osaka Municipal Technical Research Institute.
[§] Toyohashi University of Technology.
DOI: 10.1021/am900040c

Published on Web 05/01/2009

Scheme 1. Fabrication Procedure of the CeO_2 Nanostructures: (A) Preparation of the PS Sphere Template; (B) Electrodeposition of CeO_2 from $Ce(NO_3)_3$ Aqueous Solutions and Thermal Annealing

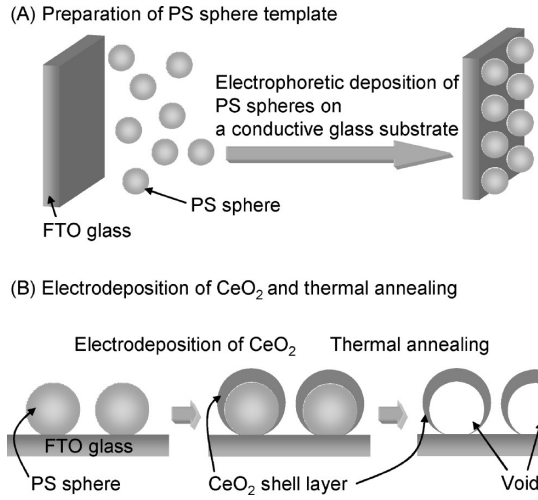

In the present paper, we report on fabrication of the PS/CeO_2 core/shell and CeO_2 hollow nanostructures by utilizing the above method. To form the CeO_2 shell, we conducted potentiostatic electrodeposition from aqueous $Ce(NO_3)_3$ solutions (16−18), and the influence of the $Ce(NO_3)_3$ concentration on the deposits was examined with X-ray diffraction (XRD) and field-emission scanning electron microscopy (FE-SEM). The structural morphology of the deposits on the PS sphere varied depending on the $Ce(NO_3)_3$ concentration. A spherical CeO_2 shell and nanopillars of $Ce(OH)_3$ on a CeO_2 shell layer were electrodeposited from 10 and 1 mM $Ce(NO_3)_3$ solutions, respectively. The corresponding unique hollow nanostructures of CeO_2 were obtained by thermal annealing. A possible mechanism to explain the concentration-dependent variation of the deposits was also discussed.

EXPERIMENTAL SECTION

Preparation of CeO_2 Nanostructures. Monodispersed anionic PS spheres with a diameter of ca. 400 nm (solid content of ~6 wt %) were synthesized by a soap-free emulsion polymerization method, as we have already reported in the literature (15, 19).

As shown in Scheme 1, the PS sphere template was formed by EPD in an aqueous dispersion containing 0.1 wt % PS spheres and 1.0 mM (M = mol dm^{-3}) KNO_3 at room temperature on F-doped SnO_2-coated glass (FTO glass, ~9 Ω/square, Asahi Glass, 15 mm × 30 mm × 1.1 mm). EPD was carried out at an applied voltage of 5 V for 3 min by using a direct-current (dc) power source (regulated dc power supply PA250-0.25B, Kenwood) and a conventional two-electrode cell with the FTO glass as an anode and a Pt sheet as a counter electrode. Prior to EPD, the FTO glass was ultrasonically washed with acetone and anodically polarized in a 1 M NaOH aqueous solution and was then rinsed with deionized water.

Electrodeposition of CeO_2 was performed using the resulting PS sphere template on the FTO glass as a working electrode. A Pt sheet and a Ag/AgCl electrode immersed in a saturated KCl aqueous solution were used as counter and reference electrodes, respectively. Potentiostatic electrolysis of two different $Ce(NO_3)_3 \cdot 5.7H_2O$ aqueous solutions with concentrations of 1 and 10 mM was carried out using a potentiostat (potentiostat/galvanostat HA-301, Hokuto Denko) at −0.8 V vs Ag/AgCl for an electric charge of 0.05−0.25 C cm^{-2} at 333 K without stirring. All solutions were prepared with reagent-grade chemicals and deionized water purified by a Mill-RX12 Plus system (Millipore). Thermal annealing of the deposits was carried out for 1 h at 673 K under an ambient atmosphere.

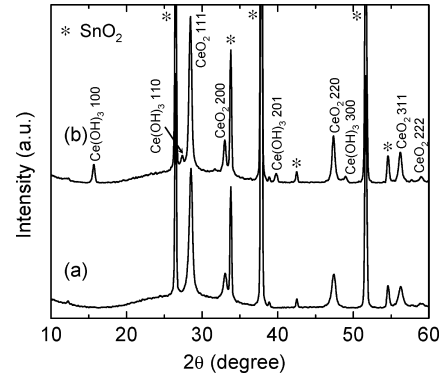

FIGURE 1. XRD patterns of electrodeposits prepared on the PS sphere templates from (a) 10 and (b) 1 mM $Ce(NO_3)_3$ solutions.

Characterization of CeO_2 Nanostructures. $\theta-2\theta$ XRD measurements were performed using a Rigaku RINT 2500 system with monochromated Cu Kα radiation generated at 40 kV and 200 mA. A field-emission scanning electron microscope (JEOL JSM-6700F) was used for the observation of structural morphologies.

RESULTS AND DISCUSSION

Structure. Figure 1 shows XRD patterns of deposits formed on the PS sphere templates from 10 and 1 mM $Ce(NO_3)_3$ solutions. On the patterns of deposits from a 10 mM $Ce(NO_3)_3$ solution (Figure 1a), all peaks were identified as those for CeO_2 with a cubic structure (2θ = 28.5°, 33.0°, 47.4°, 56.3°, and 58.9°) and SnO_2 with a tetragonal structure, which is derived from the FTO glass substrate (20). No peaks assignable to Ce^{III} compounds, such as Ce_2O_3 and $Ce(OH)_3$, were recognized on the pattern. In contrast, some peaks assigned to $Ce(OH)_3$ with a hexagonal structure (2θ = 15.7°, 27.4°, 39.8°, and 49.0°) were observed on the patterns of deposits from a 1 mM $Ce(NO_3)_3$ solution along with the diffraction peaks of CeO_2 and SnO_2 (Figure 1b). Regardless of the $Ce(NO_3)_3$ concentrations, the cubic lattice constants of CeO_2 calculated from the peak angles were 5.420 Å, which was slightly larger than the value (5.411 Å) tabulated in the ICDD card (20). It has already been reported that the Ce^{3+} ion has a larger ionic radius (1.15 Å) than that of the Ce^{4+} ion (1.09 Å) (21), and CeO_2 lattice expansion due to incorporation of the Ce^{3+} ions was observed (22, 23). Therefore, expansion of the CeO_2 lattice observed here can be attributed to incorporated Ce^{3+} ions. The hexagonal lattice constant of $Ce(OH)_3$ deposited from the 1 mM $Ce(NO_3)_3$ solution was estimated to be 3.799 Å in the *a* axis and 6.499 Å in the *c* axis. Compared to the standard value of 3.82 Å in the *a* axis and 6.5 Å in the *c* axis, this lattice reduction is also probably due to incorporation of the Ce^{4+} ions into the hexagonal $Ce(OH)_3$ (24).

These deposits were annealed at 673 K for 1 h under an ambient atmosphere. Their XRD patterns were almost the same as that before annealing in profile and peak angles (2θ

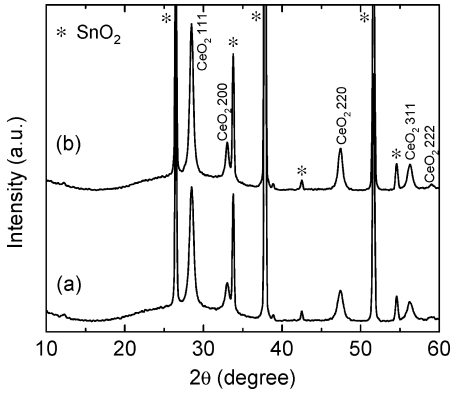

FIGURE 2. XRD patterns of electrodeposits prepared on the PS sphere templates from (a) 10 and (b) 1 mM $Ce(NO_3)_3$ solutions and annealed at 673 K for 1 h under an ambient atmosphere.

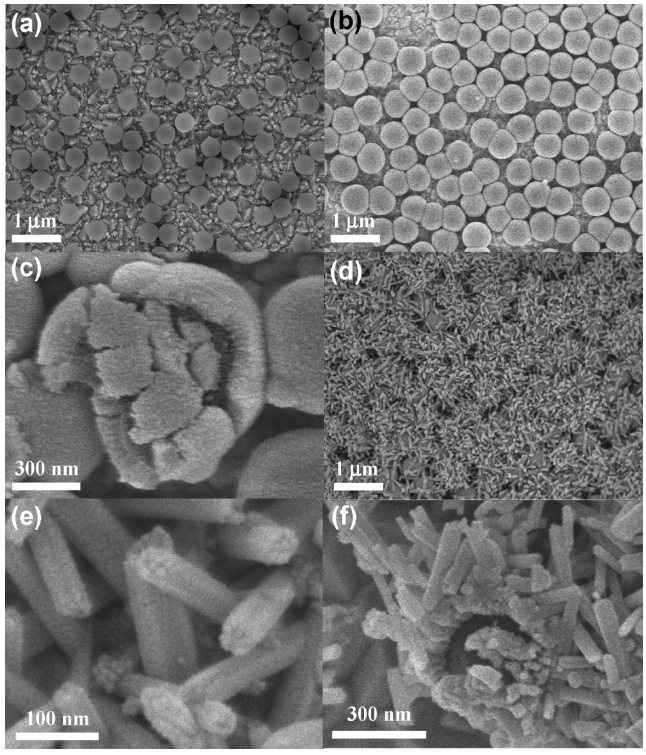

FIGURE 3. FE-SEM images of (a) a PS sphere template and (b−f) CeO_2 nanostructures electrodeposited on the PS sphere templates from (b) 10 and (d) 1 mM $Ce(NO_3)_3$ solutions. Parts c and e/f are magnified images of parts b and d, respectively.

= 28.5°, 33.0°, 47.5°, 56.2°, and 59.3° in Figure 2a and θ = 28.5°, 33.0°, 47.5°, 56.3°, and 59.0° in Figure 2b), except for the disappearance of the $Ce(OH)_3$ peaks. This means that the annealing at 673 K for 1 h gave the transformation of $Ce(OH)_3$ to CeO_2. The lattice constants of CeO_2 electrodeposited from 10 and 1 mM $Ce(NO_3)_3$ solutions increased to 5.414 and 5.417 Å, respectively, by the annealing and approached the standard value (5.411 Å) (20), indicating that the incorporated Ce^{3+} was oxidized to Ce^{4+}.

Morphology. Figure 3 shows FE-SEM images of the PS sphere template before and after electrodeposition of CeO_2 from 10 and 1 mM $Ce(NO_3)_3$ solutions at an electric charge of 0.25 C cm^{-2}. As shown in Figure 3a, a PS sphere monolayer was observed on a FTO glass substrate without aggregation and accumulation. The adsorption density of the PS spheres was estimated from the FE-SEM image to be about 3 spheres μm^{-2}.

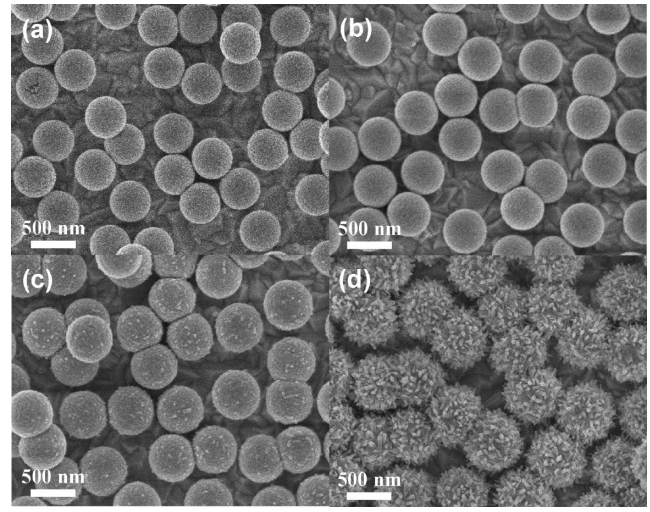

FIGURE 4. Surface FE-SEM images of nanostructures electrodeposited on the PS sphere templates at an electric charge of (a) 0.05, (b) 0.1, (c) 0.15, and (d) 0.2 C cm^{-2} from 1 mM $Ce(NO_3)_3$ solutions.

After electrodeposition of CeO_2, the structural morphology of the deposits depended on the $Ce(NO_3)_3$ concentration. From a 10 mM $Ce(NO_3)_3$ solution (Figure 3b), spherelike nanostructures consisting of the PS sphere core and CeO_2 shell with a diameter of ca. 700 nm were formed. The thickness of the CeO_2 shell could be estimated to be 100−150 nm, as shown in an accidentally cracked nanostructure (Figure 3c). On the other hand, needlelike nanostructures were formed from a 1 mM $Ce(NO_3)_3$ solution. Needles with 200−300 nm length and 30−50 nm width were randomly deposited, as seen in Figure 3d,e. As shown in an accidentally cracked nanostructure (Figure 3f), a dense shell layer could be seen between the needles and the PS sphere core. This implies that the nanostructure obtained from a 1 mM $Ce(NO_3)_3$ solution consists of the shell layer covering the PS sphere surface and many needles on the shell layer. From the XRD pattern of the deposit from a 1 mM $Ce(NO_3)_3$ solution (Figure 1b), the deposit is expected to contain both CeO_2 and $Ce(OH)_3$.

In order to identify the constituents and the formation pathway of the needles and the shell layer on the PS sphere core, electrodeposition from a 1 mM $Ce(NO_3)_3$ solution was carried out at some different electric charges (0.05−0.2 C cm^{-2}). Figure 4 shows FE-SEM images of the resulting nanostructures. Spherelike nanostructures (Figure 4a,b) with ca. 500 nm diameter were obtained for an electric charge of 0.05 or 0.1 C cm^{-2}, and then one can observe needles deposited on the surface of the spherelike nanostructures for an electric charge of 0.15 or 0.2 C cm^{-2} (Figure 4c,d). This clearly shows that the shell layer formed on the PS sphere surface at the early stage of electrodeposition and, subsequently, the needles deposited on the shell surface. Also, on the XRD pattern of the nanostructures electrodeposited at an electric charge of 0.1 C cm^{-2}, no peaks assignable to hexagonal $Ce(OH)_3$ could be seen. Therefore, the shell layer on the PS sphere surface and the needles on

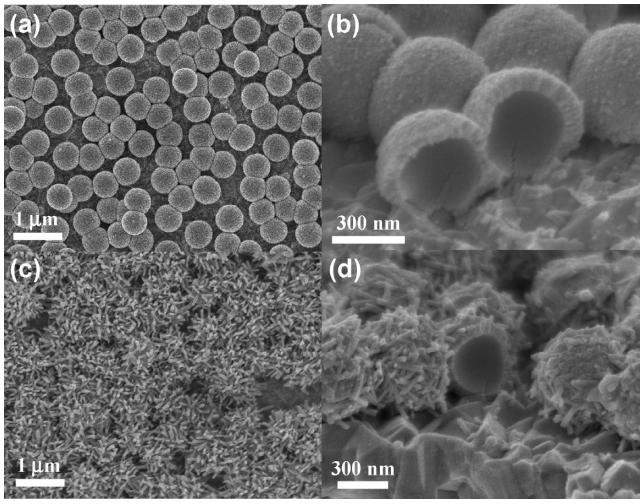

FIGURE 5. FE-SEM images of CeO_2 nanostructures electrodeposited on the PS sphere templates from (a and b) 10 and (c and d) 1 mM $Ce(NO_3)_3$ solutions and annealed at 673 K for 1 h under an ambient atmosphere.

the shell are identified as CeO_2 and $Ce(OH)_3$, respectively. While the species deposited from a 1 mM $Ce(NO_3)_3$ solution depended on the electric charge, the spherelike CeO_2 shell layer kept growing with increasing electric charges in a 10 mM $Ce(NO_3)_3$ solution without deposition of $Ce(OH)_3$ needles. This drastic change of morphology and deposition species during electrodeposition has occurred only in a 1 mM solution. The cause of the different deposits is mentioned hereinafter.

From Figures 3 and 4, it was observed that CeO_2 was electrodeposited only on the PS sphere surface but not on the FTO substrate surface. A reason for selective deposition of CeO_2 is interaction between cationic cerium species and a sulfate group that is immobilized on the PS sphere surface, as confirmed in the case of ZnO electrodeposition on the PS sphere (15). Similarly, $Ce(OH)_3$ needles were formed only on the CeO_2 shell surface not on the FTO surface (Figure 4), probably because the CeO_2 shell plays a role as a nucleus for the growth of $Ce(OH)_3$ needles.

Figure 5 shows FE-SEM images of CeO_2 nanostructures electrodeposited from 10 and 1 mM $Ce(NO_3)_3$ solutions and annealed at 673 K for 1 h under an ambient atmosphere. The annealing of deposits resulted in CeO_2 hollow nanostructures by decomposition of the PS sphere core, and no apparent cracks on the hollow spheres were recognized. The $Ce(OH)_3$ needles were transformed into CeO_2 needles by oxidation and dehydration while maintaining the needlelike structure. One can therefore prepare the spherelike and needlelike nanostructures of CeO_2 selectively by the choice of the $Ce(NO_3)_3$ concentration. The resulting hollow nanostructure with CeO_2 nanopillars is unique and can be expected for broad applications such as photocatalysts, fuel cells, and photovoltaic cells because of the high specific surface area.

Deposition Mechanism. Electrodeposition mechanisms of CeO_2 from simple cerium salt solutions have been elaborated in a number of papers (17, 25, 26) and proposed as follows: (17):

$$O_2 + 2H_2O + 2e^- \rightarrow H_2O_2 + 2OH^- \qquad E^0 = +2.05\ \text{V vs Ag/AgCl} \quad (1)$$

$$2Ce^{3+} + 2OH^- + H_2O_2 \rightarrow 2Ce^{IV}(OH)_2{}^{2+} \quad (2)$$

$$Ce^{IV}(OH)_2{}^{2+} + 2OH^- \rightarrow Ce^{IV}O_2 + 2H_2O \quad (3)$$

with an overall net reaction of

$$2Ce^{3+} + 4OH^- + O_2 + 2e^- \rightarrow 2CeO_2 + 2H_2O \quad (4)$$

When a $Ce(NO_3)_3$ solution is employed as in this study, the reduction of nitrate ions to nitrite ions, which gives hydroxide ions, is also possible.

$$NO_3{}^- + H_2O + 2e^- \rightarrow NO_2{}^- + 2OH^- \qquad E^0 = -0.189\ \text{V vs Ag/AgCl} \quad (5)$$

Generation of hydroxide ions by reduction of dissolved oxygen (eq 1) and/or nitrate ions (eq 5) raises the pH in the vicinity of a working electrode. Hydrogen peroxide oxidizes Ce^{3+} to form an intermediate of $Ce^{IV}(OH)_2{}^{2+}$ (eq 2). $Ce^{IV}(OH)_2{}^{2+}$ is precipitated as insoluble CeO_2 through a reaction with OH^- ions and dehydration (eq 3).

Although a reason for generation of the $Ce(OH)_3$ needles from the lower $Ce(NO_3)_3$ concentration is not clear at present, we propose a possible mechanism based on the results here. At first, the influence of the NO_3^- ions on electrodeposition of CeO_2 was examined. From 10 and 1 mM $CeCl_3$ solutions, similar spherelike and needlelike structures were electrodeposited, respectively, as shown in Figure 6. Moreover, on an XRD pattern of the deposit from the 10 mM $CeCl_3$ solution, all peaks were identified as those for CeO_2 and SnO_2, while some peaks assigned to $Ce(OH)_3$ were observed from a 1 mM $CeCl_3$ solution. These results indicate that NO_3^- ions have no influence on the structural variation of the deposits depending on the $Ce(NO_3)_3$ concentration. For further investigation, variation of the cathodic current density during potentiostatic electrodeposition in the $Ce(NO_3)_3$ solutions was monitored (Figure 7). The current density in a 10 mM $Ce(NO_3)_3$ solution increased steadily to 0.15 mA cm^{-2} throughout the electrodeposition, while it increased up to 0.1 mA cm^{-2} after 0.4 h and remained at the value throughout electrodeposition in a 1 mM $Ce(NO_3)_3$ solution. The increase of the current density corresponds to an increase in the deposition area due to the growth of PS/CeO_2 core/shell nanostructures. On the other hand, suppression of the increasing current means stopping of the

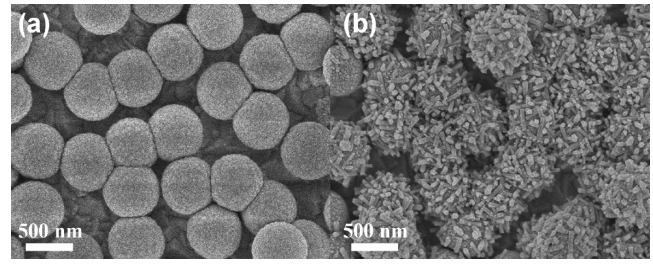

FIGURE 6. Surface FE-SEM images of CeO_2 nanostructures electrodeposited on the PS sphere templates from (a) 10 and (b) 1 mM $CeCl_3$ solutions.

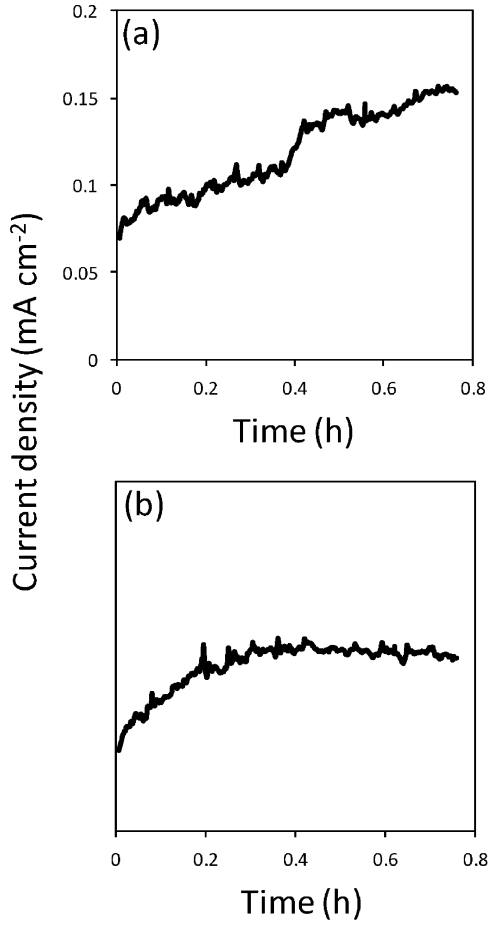

FIGURE 7. Current density variations for electrodeposition of CeO_2 at −0.8 V vs Ag/AgCl from (a) 10 and (b) 1 mM $Ce(NO_3)_3$ solutions.

CeO_2shell growth and the onset of deposition of $Ce(OH)_3$ needles that have an almost constant growth front. In fact, the changing point at a deposition time of 0.4 h (Figure 7) was estimated to correspond to an electric charge of 0.126 C cm^{-2}; this value lies between the electric charges in the experiment of Figure 4b.c. From the viewpoint of the overall net reaction (eq 4), such a threshold of the current density for the CeO_2 growth probably involves a diffusion-limited behavior of Ce^{3+} with lower concentration. Because electroreduction of oxygen (eq 1) is continued regardless of the limited supply of Ce^{3+}, hydrogen peroxide results in an oversupply. Then the following decomposition of hydrogen peroxide to hydroxide ions is induced because hydrogen peroxide is unstable under the reductive condition (27).

$$H_2O_2 + 2e^- \rightarrow 2OH^- \quad E^0 = +1.98 \text{ V vs Ag/AgCl} \tag{6}$$

If this competitive reaction (eq 6) dominates over oxidation of Ce^{3+} (eq 2), CeO_2 can no longer be deposited, and alternatively a thermodynamically stable precipitate of $Ce(OH)_3$ is generated (28).

$$Ce^{3+} + 3OH^- \rightarrow Ce(OH)_3 \tag{7}$$

CONCLUSIONS

Two types of core/shell nanostructures of PS/CeO_2 have been prepared by electrodeposition on the PS sphere template from $Ce(NO_3)_3$ aqueous solutions. Electrodeposition in 10 and 1 mM $Ce(NO_3)_3$ solutions gave the spherical CeO_2 and needlelike $Ce(OH)_3/CeO_2$ shells, respectively. The needlelike $Ce(OH)_3/CeO_2$ shells were composed of a large number of $Ce(OH)_3$ needles formed on CeO_2 shell layers, indicating that the deposit species changes from CeO_2 to $Ce(OH)_3$ during electrodeposition within the applied electric charge range of 0.1−0.15 C cm^{-2} only in a 1 mM Ce^{3+} solution. Further experiments to investigate the deposition mechanism supported that a diffusion-limited behavior of Ce^{3+} ions caused by an increase in the deposition area is a key for understanding the concentration-dependent structural variation of the deposits. Deposition of $Ce(OH)_3$ would begin when electrogenerated hydrogen peroxide was consumed by decomposition under reductive condition and could no longer oxidize Ce^{3+} ions. The thermal annealing of these core/shell nanostructures at 673 K led to the elimination of the PS core and the transformation of $Ce(OH)_3$ to CeO_2 while keeping their original shapes, giving the two corresponding types of CeO_2 hollow shells. By the method employed here, CeO_2 nanostructures with selective morphology and high surface area were fabricated directly on the conductive substrate. Thus, the obtained unique nanostructures are expected to be a promising functional electrode material for catalytic applications including photocatalysts, sensors, and fuel cells.

Acknowledgment. This work was supported by the R&D for Next Generation PV Systems Program of the Incorporated Agency New Energy and Industrial Development Organization under the Ministry of Economy, Trade and Industry of Japan.

REFERENCES AND NOTES

(1) Feng, X. D.; Sayle, D. C.; Wang, Z. L.; Paras, M. S.; Santora, B.; Sutorik, A. C.; Sayle, T. X. T.; Yang, Y.; Ding, Y.; Wang, X.; Her, Y.-S. *Science* **2006**, *312*, 1504.
(2) Lunderg, M.; Skaerman, B.; Cesar, F.; Wallenberg, L. R. *Microporous Mesoporous Mater.* **2002**, *54*, 97.
(3) Jasinski, P.; Suzuki, T.; Anderson, H. U. *Sens. Actuators B* **2003**, *95*, 73.
(4) Zhang, Y.; Si, R.; Liao, C.; Yan, C. *J. Phys. Chem. B* **2003**, *107*, 10159.
(5) Bamwenda, G. R.; Uesugi, T.; Abe, Y.; Sayama, K.; Arakawa, H. *Appl. Catal., A* **2001**, *205*, 117.
(6) Nair, J. P.; Wachtel, E.; Lubomirsky, I.; Fleig, J.; Maier, J. *Adv. Mater.* **2003**, *15*, 2077.
(7) Yang, S.; Gao, L. *J. Am. Chem. Soc.* **2006**, *128*, 9330.
(8) Vantomme, A.; Yuan, Z.-Y.; Du, G.; Su, B.-L. *Langmuir* **2005**, *21*, 1132.
(9) Zhou, K.; Yang, Z.; Yang, S. *Chem. Mater.* **2007**, *19*, 1215.
(10) Waterhouse, G. I. N.; Metron, J. B.; Idriss, H.; Sun-Waterhouse, D. *Chem. Mater.* **2008**, *20*, 1183.
(11) Yuan, J.; Laubernds, K.; Zhang, Q.; Suib, S. L. *J. Am. Chem. Soc.* **2003**, *125*, 4966.
(12) Li, H.; Bian, Z.; Zhu, J.; Zhang, D.; Li, G.; Huo, Y.; Li, H.; Lu, Y. *J. Am. Chem. Soc.* **2007**, *129*, 8406.
(13) Titirici, M.-M.; Antonietti, M.; Thomas, A. *Chem. Mater.* **2006**, *18*, 3808.
(14) Chen, C.-H.; Abbas, S. F.; Morey, A.; Sithambaram, S.; Xu, L.-P.; Garces, H. F.; Hines, W. A.; Suib, S. L. *Adv. Mater.* **2008**, *20*, 1205.
(15) (a) Watanabe, M.; Aritomo, H.; Yamaguchi, I.; Shinagawa, T.; Tamai, T.; Tasaka, A.; Izaki, M. *Chem. Lett.* **2007**, *36*, 680. (b) Izaki, M.; Watanabe, M.; Aritomo, H.; Yamaguchi, I.; Asahina, S.; Shinagawa, T.; Chigane, M.; Inaba, M.; Tasaka, A. *Cryst. Growth Des.* **2008**, *8*, 1418.

(16) Li, F. B.; Thompson, G. E. *J. Electrochem. Soc.* **1999**, *146*, 1809.
(17) Aldykiewicz, A. J.; Davenport, A. J.; Isaacs, H. S. *J. Electrochem. Soc.* **1996**, *143*, 147.
(18) Switzer, J. A. *Am. Ceram. Soc. Bull.* **1987**, *66*, 1521.
(19) Warson, H.; Finch, C. A. *Applications of Synthetic Resin Lattices*; John Wiley & Sons: New York, 2001; Vol 1.
(20) *Joint Committee of Powder Diffraction Standard, Powder Diffraction File, No. 34-0394*; International Centre for Diffraction Data, Newtown Square, PA, 1992.
(21) Jenkins, R.; Snyder, R. L. In *Introduction to X-Ray Powder Diffractometry*; Wiley-InterScience: New York, 1996; p 89.
(22) Shannon, R. D.; Prewitt, C. T. *Acta. Crystallogr. B* **1969**, *25* 925.
(23) Ho, C.; Yu, J. C.; Kwong, T.; Mak, A. C.; Lai, S. *Chem. Mater.* **2005**, *17*, 4514.
(24) *Joint Committee of Powder Diffraction Standard, Powder Diffraction File, No. 19-0284*; International Centre for Diffraction Data, Newtown Square, PA, 1992.
(25) Li, F.-B.; Newman, R. C.; Thompson, G. E. *Electrochim. Acta* **1997**, *42*, 2455.
(26) Scholes, F. H.; Soste, C.; Hughes, A. E.; Hardin, S. G.; Curtis, P. R. *Appl. Surf. Sci.* **2006**, *253*, 1770.
(27) Pourbaix, M. *Atlas of Electrochemical Equilibtia in Aqueous Solutions*; NACE: Houston, TX, 1974; p 542.
(28) Pourbaix, M. *Atlas of Electrochemical Equilibtia in Aqueous Solutions*; NACE: Houston, TX, 1974; p 192.

AM900040C